Proton imaging of hohlraum plasma stagnation in inertial-confinement-fusion experiments

2013 Nucl. Fusion 53 073022

(http://iopscience.iop.org/0029-5515/53/7/073022)

Nucl. Fusion **53** (2013) 073022 (6pp) doi:10.1088/0029-5515/53/7/073022

Proton imaging of hohlraum plasma stagnation in inertial-confinement-fusion experiments

C.K. Li[1], F.H. Séguin[1], J.A. Frenje[1], N. Sinenian[1], M.J. Rosenberg[1], M.J.-E Manuel[1], H.G. Rinderknecht[1], A.B. Zylstra[1], R.D. Petrasso[1], P.A. Amendt[2], O.L. Landen[2], A.J. Mackinnon[2], R.P.J. Town[2], S.C. Wilks[2], R. Betti[3], D.D. Meyerhofer[3], J.M. Soures[3], J. Hund[4], J.D. Kilkenny[4] and A. Nikroo[4]

[1] Plasma Science and Fusion Center, Massachusetts Institute of Technology, Cambridge, MA 02139, USA
[2] Lawrence Livermore National Laboratory, Livermore, CA 94550, USA
[3] Laboratory for Laser Energetics, University of Rochester, Rochester, NY 14623, USA
[4] General Atomics, San Diego, CA 92186, USA

Received 4 December 2012, accepted for publication 14 May 2013
Published 11 June 2013
Online at stacks.iop.org/NF/53/073022

Abstract
Proton radiography of the spatial structure and temporal evolution of plasma blowing off from a hohlraum wall reveals how the fill gas compresses the wall blow-off, inhibits plasma jet formation and impedes plasma stagnation in the hohlraum interior. The roles of spontaneously generated electric and magnetic fields in hohlraum dynamics and capsule implosions are demonstrated. The heat flux is shown to rapidly convect the magnetic field due to the Nernst effect, which is shown to be ∼10 times faster than convection by the plasma fluid from expanded wall blow-off ($v_N \sim 10v$). This leads to inhibition of heat transfer from the gas region in the laser beam paths to the surrounding cold gas, resulting in a local plasma temperature increase. The experiments show that interpenetration of the two materials (gas and wall) occurs due to the classical Rayleigh–Taylor instability as the lighter, decelerating ionized fill gas pushes against the heavier, expanding gold wall blow-off. This experiment provides physics insight into the effects of fill gas on x-ray-driven implosions, and would impact the ongoing ignition experiments at the National Ignition Facility.

(Some figures may appear in colour only in the online journal)

1. Introduction

Achieving ignition and high gain is the ultimate goal of inertial confinement fusion (ICF) [1–5], which requires that a cryogenic deuterium–tritium (DT) filled spherical capsule be symmetrically imploded to reach sufficiently high temperature and density. The symmetry requirements impose strict constraints for achieving fusion ignition [1–9]. The tolerable drive asymmetry of an implosion, in a time-integrated sense, is less than 1–2%, depending on the ignition margin [3–6]. In the indirect-drive approach to ICF, the capsule implodes in response to a quasi-uniform hohlraum radiation field with minimal high-mode-number non-uniformities [3–9]; low-mode-number implosion asymmetries consequently become a major challenge. An example of such an asymmetry would be a time-integrated P_2 (second-order Legendre polynomial) non-uniformity that could lead to different radial velocities and densities between the pole and equator, converting less kinetic energy into internal energy than for a symmetric implosion and resulting in a higher drive energy required for ignition.

A high-Z plasma (e.g. gold) from wall blow-off, which can cause motion of the laser absorption region and alter the spatial distribution of x-ray energy sources and sinks, has been shown to cause low-mode-number implosion asymmetries [3–9]. The blow-off quickly fills the interior of an initially empty hohlraum, leading to early on-axis plasma stagnation [3–9]. The stagnated plasma has a high pressure and can asymmetrically compress the capsule.

Motion of the laser-deposition (x-ray emission) region must be minimized to achieve the required drive symmetry. Two approaches that have been proposed for doing this [3, 4] are (1) coating the hohlraum wall with a low-Z liner and

(2) filling the hohlraum interior with a low-Z gas. Neither the liner nor the fill gas stops the wall blow-off, but they suppress the low-density plasma wall blow-off. In the first approach, plasma jets are formed due to the interaction of pairs of adjacent, expanding plumes of low-Z liner blow-off [3–5, 9]. The radially moving jets are supersonic and quickly stagnate at the hohlraum axis, potentially resulting in asymmetries in drive that may impact the capsule implosion. The ignition campaign at the National Ignition Facility (NIF) [10] currently adopts the second approach [3–9]. Hohlraums are filled with helium-4 gas [5, 6] at 0.96 mg cm^{-1} (when fully ionized, $n_e \sim 0.03 n_{crit}$, where n_{crit} is the critical electron density for 0.35 μm laser light). The gas is confined in the hohlraum by thin polyimide windows over the pair of laser entrance holes (LEHs).

Implosion symmetry and dynamics have been studied experimentally with a number of diagnostics. Conventional x-ray imaging (utilizing either x-ray backlighting or x-ray self-emission [6–8]) is very useful, but does not provide information about self-generated electric (E) and magnetic (B) fields and their effects on hohlraum drive symmetry. Radiographs made with charged particles, on the other hand, do provide direct information about fields as well as the plasma spatial distribution.

This paper presents proton-radiography-based observations showing that gas fill impedes hohlraum plasma stagnation. The radiography technique is outlined in section 2, while radiographs of hohlraum plasma stagnation are presented in section 3. The underlying physics of the measured images are discussed in section 4, and the main results are summarized in section 5.

2. Proton radiography of laser-driven hohlraums

Imaging plasma using an external backlighter source of radiation or particles provides important information that is different from that obtained by imaging plasma self-emission. In ICF experiments, for example, x-ray backlighting has been widely used to diagnose plasma conditions associated with variations of density and temperature such as those due to hydrodynamic instabilities and shock wave propagation [3–5, 11, 12]. Proton radiography has been developed as another important diagnostic method for probing plasmas, because it is sensitive both to density and to electromagnetic fields [9, 13–19]. Fields can be inferred through the deflections they induce in proton trajectories. Recent works [9, 13–19] have demonstrated that high-resolution images containing deflection information can be obtained. In these experiments, backlighter protons were generated either by irradiating a solid metal target with a high-intensity petawatt laser beam (which produces a large proton flux and a continuous energy spectrum of up to ~50 MeV) [20–27] or by imploding an ICF capsule filled with D^{3}He (which produces monoenergetic fusion protons) [13].

This paper uses the latter approach, which has distinct quantitative spectral advantages over radiography with broadband proton sources. The backlighting protons were either directed along the hohlraum axis, through the LEHs, for an end-on view of the plasma, or passed through the hohlraum walls, to probe the spatial structure and temporal evolution of the hohlraum plasma flow and associated spontaneous fields

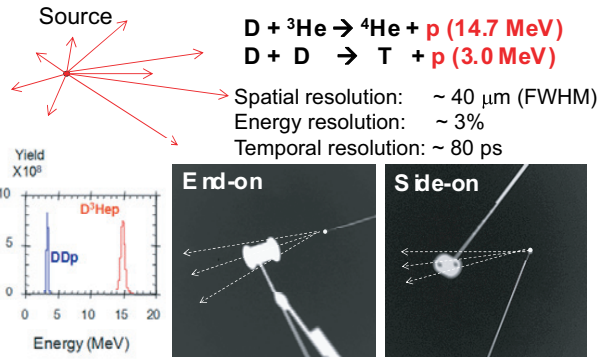

Figure 1. Experimental setup for end-on and side-on proton radiography. A backlighter (imploded D^{3}He-filled, thin-glass-shell capsule driven by 30 OMEGA laser beams) is 1 cm from the hohlraum centre. It provides the illustrated monoenergetic proton spectra from the reactions D+^{3}He $\rightarrow \alpha$ + p (14.7 MeV) and D + D $\rightarrow$ T + p (3.0 MeV). The proton positions and energies are recorded with a CR-39 detector, which is not shown here.

from the side-on direction perpendicular to the hohlraum axis. Both configurations in experiments at OMEGA [28] are illustrated in figure 1. With our CR-39 detector system [13, 29], high-resolution, time-gated, single-energy proton radiography images are obtained and allow precise connections between the experimental data and computer simulations. The monoenergetic protons used are 14.7 MeV D^{3}He protons and 3 MeV DD protons that are fusion products of the nuclear reactions occurring in an imploded capsule filled with D^{3}He gas [13, 29].

To model the spatial structure and temporal evolution of B fields generated during the laser–hohlraum interaction, two-dimensional hydrodynamic simulations were performed with LASNEX [30, 31]. Figure 2 shows the calculated B fields accompanying plasma plumes (wall blow-off) and the trajectories of the backlighting protons used to produce end-on images with information about the field dynamics. Since the dominant B field has a toroidal configuration around an expanded, annular plasma shell, the end-on protons encounter two regions containing $\boldsymbol{B}$ fields with opposite signs (figure 2), $\boldsymbol{B}_1$ and $\boldsymbol{B}_2$, as they pass through the two sides of a laser-generated plume. The deflections in the two regions do not quite cancel because the trajectories of the protons are not exactly parallel to the axis of the hohlraum, so the B field differential sampled by the transiting proton $\delta B = |\boldsymbol{B}_2| - |\boldsymbol{B}_1|$ is not zero. Figure 3 gives the simulated spatial structure and strength of a typical B field generated near a hohlraum wall, and shows how a backlighting proton's trajectory changes after passing through the field region (the proton deflections were simulated with LSP [32]).

Figure 4 provides detailed proton-image simulations of end-on radiography of the hohlraum assuming backlighting with 14.7 MeV protons. To clearly quantify the proton trajectory deflection, a nickel mesh (60 μm thick, with a 150 μm hole-to-hole spacing and 75 μm holes) divided the backlighter protons into discrete beamlets before they passed through the hohlraum. The B fields can be estimated from the net linear displacement ξ of the beamlets in an image, relative to where they would be without the distortion, together with the geometry of the imaging system and the scale length ($L_B \equiv B/\nabla B$) [13, 16].

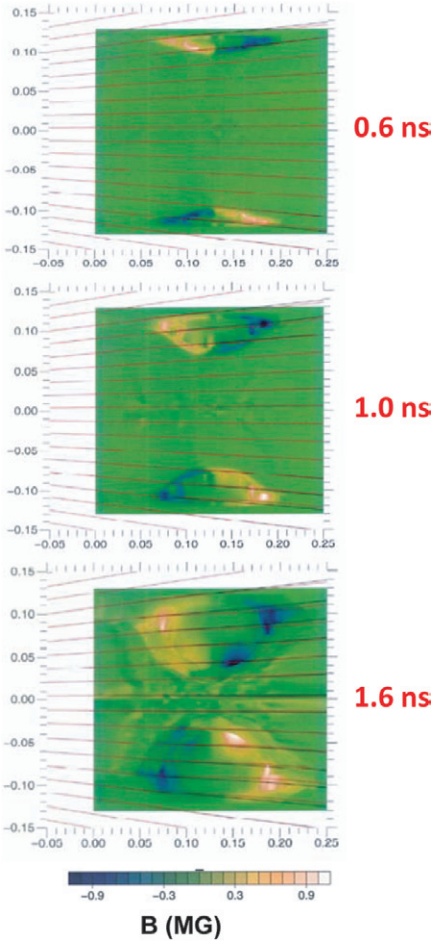

Figure 2. LASNEX-simulated B fields on an expanding annular shell surrounding the ablative plasma plumes (hohlraum wall blow-off) at different times. The solid red lines represent the trajectories of end-on backlighting protons in the experimental configuration shown in figure 1 (but with the backlighter at the left). The protons travel from left to right in the plane of this field map, and the maximum angular deflections would be for trajectories passing through the plasma plume edges.

Figure 5 shows sequences of proton end-on and side-on images obtained on different shots, covering a time period from the end of the 1 ns laser pulse, ∼2 ns after the laser pulse ended. The experiments were performed at the OMEGA laser facility, where each hohlraum was driven by 30 0.351 μm-wavelength laser beams with a total energy of ∼11 kJ in a 1 ns square pulse. The laser beams had full spatial and temporal smoothing [33]. While the proton fluence shows large variations (figure 5), the mean proton energy shows less spatial variation [9, 18]. This suggests that the trajectories of these backlighting protons are affected primarily by fields rather than by proton scattering in the plasma, because Coulomb interactions are always accompanied by energy loss [34].

3. Impeding hohlraum plasma stagnation

Figure 6 displays fluence images made with 14.7 MeV-proton backlighting of an Au hohlraum filled with ∼0.4 atm neopentane gas (C_5H_{12}) and containing a CH capsule (30 μm-thick, 550 μm-diameter plastic shell filled with 50 atm

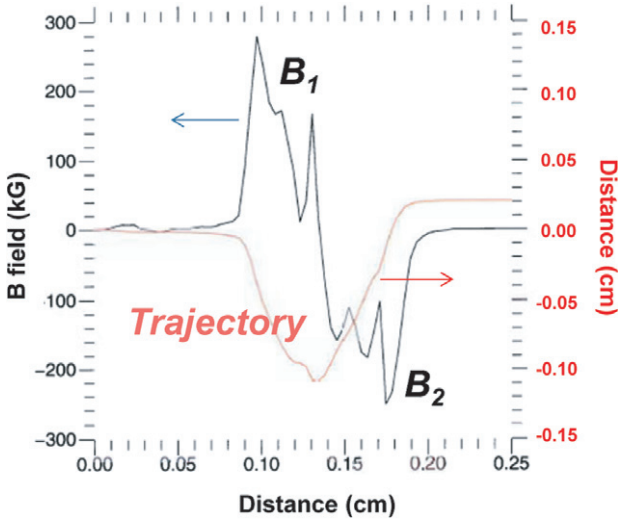

Figure 3. Trajectory of a 14.7 MeV proton travelling through the B-field region simulated by LASNEX-LSP for the experimental conditions illustrated in figures 1 and 2, showing net deflections due to non-zero overall B fields ($\delta B = |B_2| - |B_1|$).

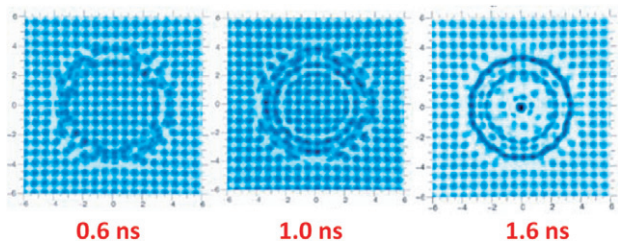

Figure 4. End-on radiographic images of laser-driven hohlraum simulated by LASNEX-LSP for the experimental conditions illustrated in figures 1 and 2, showing proton deflections due to the B fields generated by laser–wall interactions in the hohlraum at different times and for 14.7 MeV D^3He protons. The backlighting protons were assumed to be divided into beamlets by a mesh before impinging on the hohlraum.

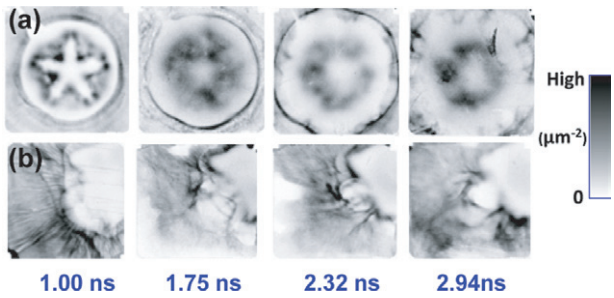

Figure 5. End-on (a) and side-on (b) proton fluence radiographs of laser-driven hohlraums made with 3 MeV protons. Within each image, darker means higher proton fluence, and the capsule-mounting stalk appears in the upper left corner [17, 18]. The smeared spatial structures are caused by fields. These images illustrate temporal evolution of the fields, plasma flow and implosions. Note that there are no mesh grids in front of the hohlraums.

H_2 gas) [18]. The proton fluence piles up in the gaps between the two expanding plasma plumes and in the region between the imploding capsule and the expanding plasmas, forming a five-prong, asterisk-like pattern that is a consequence of the OMEGA laser beam distribution (cone 3 configuration

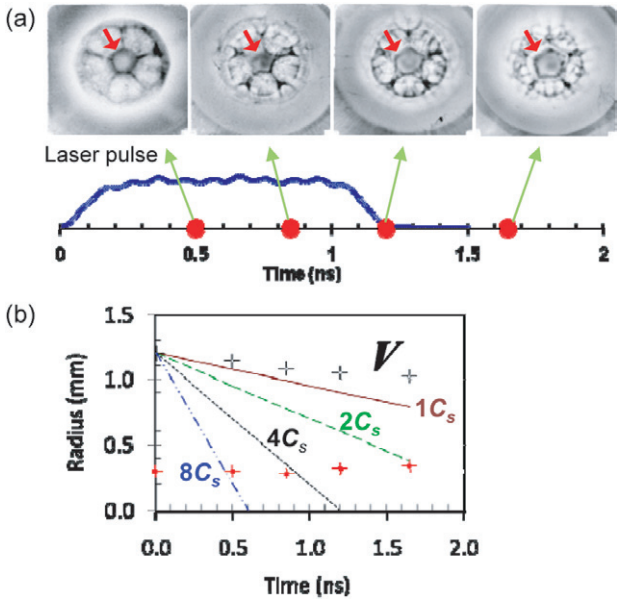

Figure 6. (*a*) End-on radiographs (made with 14.7 MeV protons) of a CH capsule imploded in a neopentane-filled hohlraum with arrows pointing to the interfaces between the Au wall blow-off and the gas plasma. (*b*) Measured interfaces between the Au wall blow-off and the gas plasma (open diamonds), and between the capsule and the gas plasma (solid squares), are compared to motion at multiples of the sound speed. The boundary position showing at ∼0.5 ns in (*a*) suggests that the hot regions of the gas plasma have reached the surface of an imploding capsule at a fast speed (∼ $8C_s$). The uncertainties for sampling times were ∼90 ps (the backlighter burn duration) while for the radius they were ∼10% (the variation in image circularity). Linear fit yields the expansion speed $v \approx (2.1 \pm 0.3) \times 10^7$ cm s^{-1} (reduced $\chi^2 = 0.662$).

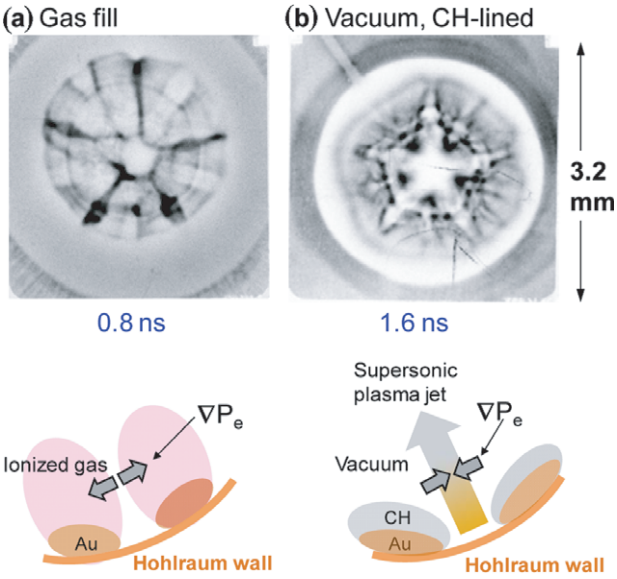

Figure 7. Proton fluence images show surpluses in the regions between the pairs of expanding plasma plumes in a gas-filled, Au hohlraum (*a*) but show deficits in a CH-lined, vacuum Au hohlraum (*b*). They indicate opposing directions of the self-generated electric fields, as illustrated schematically by the corresponding cartoons [18].

dominates). Contrary to earlier experiments that showed a deficit in proton fluence in these regions for vacuum hohlraums [9, 17], this fluence surplus suggests that no high-density plasma jets were formed. The fill gas along the laser beam path is fully ionized. The interfaces between the gas plasma and the Au wall blow-off are constrained near the wall surface. Figure 6(*b*) shows the measured radius of the interface between the Au wall plasma and the fill gas as a function of time, compared with the sound speed [$C_s \propto (ZT_e m_i^{-1})^{1/2}$] that sets the scale for hydrodynamic rarefaction expansion in vacuum [9, 17, 18]. The expansion speed of the Au blow-off is estimated to be $\sim (2.1 \pm 0.3) \times 10^7$ cm s^{-1}, which is slower than $C_s \sim 2.5 \times 10^7$ cm s^{-1}, indicating that the wall blow-off expansion has been impeded by the fill gas [18].

To explore the mechanism for forming such a unique spatial structure and its effects on impeding the hohlraum wall plasma expansion and drive dynamics, experiments were performed with solid, spherical CH targets driven in both gas-filled Au hohlraums and CH-lined vacuum Au hohlraums (figure 7). The two images show related asterisk-like structures (with spokes in the gaps between pairs of expanding plasma plumes) but with opposite proton fluence distributions: protons were focused into the gaps (high-fluence spokes) for the gas-filled hohlraum (figure 7(*a*)) but were deflected away from the spokes in the CH-lined vacuum hohlraum (figure 7(*b*)). The role of a spontaneously generated B field in these interactions can be excluded by symmetry since the toroidal B-field topology around the laser spots [9, 17, 18] cannot result in such azimuthal proton deflections. Lateral electric fields [9, 17, 18] associated with azimuthally oriented electron pressure gradients (∇P_e) in the plasma plumes and in the radial plasma jets, $E = -\nabla P_e / e n_e$, may be the source of these deflections. Another physical mechanism that could explain the deflection near the capsule before 0.5 ns is the E field associated with a supersonic heat front generated by the laser-heated gas channels that are in close proximity to the capsule. Work is in progress to quantitatively assess the relative importance of this mechanism in the generation of such a field. Since figures 7(*a*) and (*b*) show opposite deflections, E must have pointed in opposite directions.

4. Discussion

As illustrated in the cartoon in figure 7(*a*) for the gas-filled hohlraum, a high plasma pressure should have resulted from an increase in temperature inside the plasma plume and ionized gas [18]. The steep ∇P_e results in strong E fields that point laterally away from the plumes, deflecting the backlighting protons into the gaps between pairs of approaching plasma plumes. For these underdense gas plasmas ($\sim 0.03 n_{crit}$), the rapidly rising plasma temperature in the region where the laser passes results not only from continuous laser heating but from inhibition of heat flow due to the self-generated megagauss B field [8, 9, 18]; the electron thermal transport is reduced by a factor of $(1 + \omega_{ce}^2 \tau^2)^{-1}$, where ω_{ce} is the electron gyrofrequency and τ is the collision time [35, 36]. Including the contribution from magnetized window plasma, the Hall parameter $\omega_{ce}\tau$ is ∼10 [8]. The combination of inverse bremsstrahlung absorption in the Au wall and electron conduction eventually establishes a near-equilibrium plasma

condition in the laser propagation channel, and the quasi-balance of pressure leads to continuous plasma heating and temperature increase [18].

The spontaneous B field is generated initially at the hohlraum wall due to nonparallel density and temperature gradients ($\nabla n_e \times \nabla T_e$). Based on the proton deflection feature, the data in figure 6 show that the plasma temperatures were high [18] even at the earlier time (~0.5 ns) for the fully ionized, low-Z gas plasma whose front boundary already reached the surface of the imploding capsule within the region of the laser beam propagation channel; this indicates that inhibition of heat flow by fields must have taken place at an earlier time. This suggests that the transport of the field was much faster than the plasma expansion speed that carries the 'frozen in' field at high conductivity. The fluid velocity $v(< C_s)$ is too slow to explain the rapid gas plasma temperature increase at the earlier times (figures 6 and 7). Such non-local field transport must have resulted from the convection of B field with heat flux associated with 'faster' electrons due to the Nernst effect ($\propto \beta_\wedge \boldsymbol{b} \times \nabla T_e$, i.e. the current flow is driven perpendicular to a B field and ∇T_e, where $\boldsymbol{b} \equiv \boldsymbol{B}B^{-1}$ and $\beta_\wedge$ is the thermoelectric coefficient perpendicular to the B field and temperature gradient) [35, 36]. The convection velocity is approximately $v_N \approx 2q_e(5n_eT_e)^{-1}$, where $q_e = k_\perp \nabla T_e$ is the electron heat flux and $\kappa_\perp$ is the thermal conductivity. A rough estimate based on the data from figure 6 (the position of the boundary of the gas plasma that reached the surface of an imploding capsule) indicates that the lower limit for the B-field convection speed is $v_N \sim 8C_s$, suggesting that the field transport (convection) by heat flux is about one order of magnitude faster than the wall plasma expansion ($v_N \sim 10v$). The physical process of B-field generation, evolution and dissipation [$\nabla \times (D_m \nabla \times \boldsymbol{B})$] is described by Faraday's law in a plasma as [35, 36]

$$\frac{\partial \boldsymbol{B}}{\partial t} \approx -\frac{\nabla n_e \times \nabla \boldsymbol{T}_e}{e n_e} + \nabla \times (\boldsymbol{v} \times \boldsymbol{B}) - \nabla \times (\boldsymbol{D}_m \nabla \times \boldsymbol{B}) - \frac{\nabla \times \boldsymbol{R}}{e n_e}, \quad (1)$$

where D_m is the magnetic diffusion coefficient and

$$\boldsymbol{R} = \frac{(\alpha_\perp \boldsymbol{J}_\perp + \alpha_\wedge \boldsymbol{J} \times \boldsymbol{b})}{e n_e} + \beta_\perp \nabla_\perp T_e - \beta_\wedge \boldsymbol{b} \times \nabla T_e \quad (2)$$

is the contribution of electron thermal and friction forces [3, 35, 36]. The data suggest that the Nernst effect is responsible for the rapid B-field transport, which could cause a rapid gas plasma temperature increase.

The behaviour and dynamics are different in the laser-irradiated CH-lined, Au vacuum hohlraum (figure 7(*b*)). Although the ablated CH wall helps one to compress the Au blow-off, radially moving CH plasma jets are generated with the Au blow-off trailing [9, 17, 18]. This process is initiated by the CH liner ablating from the wall, which subsequently expands with the continuous arrival of wall blow-off into the region between the two adjacent expanding plumes. These plasmas collide with one another, leading to the formation of the dense plasma spokes that are redirected radially and move towards the hohlraum interior. The steep ∇P_e around the jets results in radial E fields that deflect the imaging protons away from the jets and leads to the asterisk-like spoke structure in the fluence images (figure 7(*b*)). The inward jets

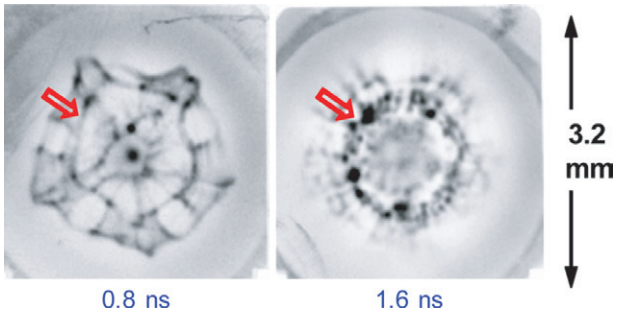

Figure 8. Proton fluence images of capsule implosions driven by gas-filled hohlraums [18]. The open arrows point at the interfaces between the Au wall blow-off and the gas plasma. A relatively smooth interface appears between the expanding wall blow-off and the ionized fill gas at time 0.8 ns, while a chaotic spatial structure and interface interpenetration are evident at time 1.6 ns. The fluence surplus inside the imploding capsule (0.8 ns) resulted from self-generated radial E fields [14, 39].

travel with supersonic speed (~$4C_s$), generating an early-time stagnation pressure that affects capsule implosion symmetry and dynamics [9, 17, 18]; this phenomenon is also observed in the pure vacuum Au hohlraum-driven experiments [9, 17].

The widths of the spokes in the images can be used with the imaging geometry to estimate the field $\int \boldsymbol{E} \times \mathrm{d}\ell \sim 3 \times 10^5$ V (where $\mathrm{d}\ell$ is the differential path length along the proton trajectory through the field area) [9, 17, 18]. A scale length of ~0.1 cm (~laser spot width) for the field in a jet spoke implies $E \sim 3 \times 10^6\ \mathrm{V\,cm^{-1}}$.

To further study the dynamics of the interface and its effect on impeding the plasma stagnation, capsule implosions were performed with a denser hohlraum gas fill (~1 atm, C_5H_{12}) at two sampling times (figure 8). A relatively smooth interface appears between the expanding wall blow-off and the ionized fill gas at 0.8 ns, while a chaotic spatial structure and interface interpenetration are evident at 1.6 ns. This interpenetration is caused by hydrodynamic instabilities and associated B fields [37, 38]. The surface perturbations that are seeded at the plume front can be amplified by the classical Rayleigh–Taylor (RT) instability occurring at the interface of the lighter, decelerating, ionized gas plasma and the heavier, expanding Au blow-off [3]. This instability has a growth rate [3] $\gamma_{RT} \approx (2\pi A_t a k)^{1/2}$, where a is the acceleration, $\sim 10^{16}\ \mathrm{cm\,s^{-2}}$ estimated from figure 6(*b*); $k = m(2\pi r)^{-1}$ is the perturbation wave number. As an example, for a mode number $m \sim 50$ at half the hohlraum radius $r \sim 0.5 \times 0.12$ cm, $k \sim 130\ \mathrm{cm^{-1}}$. The Atwood number $A_t = (\rho_2 - \rho_1)/(\rho_2 + \rho_1)$ at the interface is $A_t \approx 0.54$ (for ~$0.1n_{crit}$ the gas fill plasma has $\rho_1 \approx 3\ \mathrm{mg\,cm^{-3}}$, while the Au plasma has $\rho_2 \approx 10\ \mathrm{mg\,cm^{-3}}$). A rough estimate gives $\gamma_{RT} \sim 2.7 \times 10^9\ \mathrm{s^{-1}}$, and a perturbation would grow by a factor of ~15 in a period of 1 ns [18].

A similar interaction process occurred between the ablated capsule plasma and the gas plasma. The consequence is a reduced benefit of the gas fill because the enhanced interpenetration (or mixing) between the Au blow-off and the gas plasma leads to high-Z material stagnating earlier in the hohlraum interior. This effect does not appear to be severe, because it happens during the coasting phase when the imploding shell moves at a speed that is comparable to, or even faster than, the outward ablation speed (~C_s). At this time,

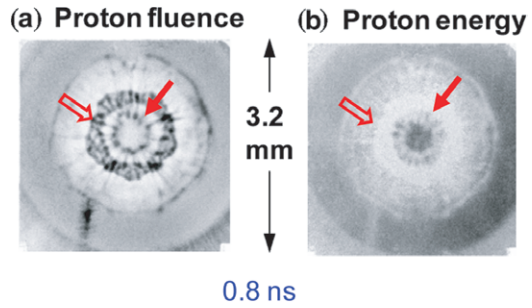

Figure 9. Images of proton fluence (*a*) and energy (*b*) (darker means lower energy) from a solid CH sphere driven by a vacuum Au hohlraum with polyimide windows. The open (solid) arrows point at the interfaces between the Au wall blow-off and the gas plasma (between the capsule ablation and gas plasma).

the high-Z blow-off should be sonically decoupled from the imploding capsule.

To explore the role of the CH windows in impeding plasma stagnation, capsules were imploded in vacuum hohlraums with CH windows on both LEHs. When laser beams pass through the LEHs, the CH windows are evaporated, ionized and magnetized. The high-pressure, low-Z window plasma rapidly flows into the hohlraum interior, filling it and altering the wall blow-off dynamics by impeding the plasma stagnation like the gas fill does. Spontaneous B fields convect with the flowing window plasma and inhibit electron thermal conduction, further increasing the plasma temperature [17, 18] and impeding the motion of the wall blow-off. Figure 9 shows radiographic images taken while the drive laser was on. Due to the inflow of CH window plasma, no plasma jets formed and the wall blow-off was contained radially. More protons deflected in the radial direction than in the lateral directions of the radially expanding plume. This is because $|\boldsymbol{L}_T| > |\boldsymbol{L}_n|$, where $\boldsymbol{L}_T = T_\mathrm{e}(\nabla T_\mathrm{e})^{-1}$ and $\boldsymbol{L}_n = n_\mathrm{e}(\nabla n_\mathrm{e})^{-1}$ are the temperature and density scale lengths, respectively, and $\boldsymbol{E} \approx |\boldsymbol{E}_r + \boldsymbol{E}_\theta| \propto n_\mathrm{e}^{-1}\nabla P_\mathrm{e} \sim T_\mathrm{e}|\boldsymbol{L}_n^{-1} + \boldsymbol{L}_T^{-1}|$, leading to $|\boldsymbol{E}_r| > |\boldsymbol{E}_\theta|$.

5. Summary

In summary, we have performed the first time-gated proton radiography showing how the spatial structure and temporal evolution of the fill gas compress the wall blow-off, inhibit plasma jet formation and impede plasma stagnation in the hohlraum interior. We have shown that plasma interpenetration due to classical Rayleigh–Taylor instabilities occurs as the lighter, decelerating ionized fill gas pushes against the heavier, expanding gold wall blow-off. The important roles that spontaneously generated E and B fields play in hohlraum dynamics and capsule implosion were discussed. The heat flux was shown to rapidly convect the B field due to the Nernst effect. This experiment provides novel physics insight into the effects of fill gas on x-ray-driven implosions, and could impact on the ignition experiments at the NIF.

Acknowledgments

This work was supported in part by the US DOE and LLE National Laser User's Facility (DE-FG52-07NA28059 and DE-FG03-03SF22691), LLNL (B543881 and LDRD-11-ER-075), LLE (414090-G), FSC (412761-G), and General Atomics (DE-AC52- 06NA 27279). A.B. Zylstra is supported by the Stewardship Science Graduate Fellowship (DE-FC52-08NA28752).

References

[1] Nuckolls J. *et al* 1972 *Nature* **239** 139
[2] McCrory R.L. *et al* 1989 *Nature* **335** 225
[3] Lindl J.D. 1999 *Inertial Confinement Fusion* (New York: Springer)
[4] Atzeni S. and Meyer-Ter-Vehn J. 2004 *The Physics of Inertial Fusion* (Oxford: Clarendon)
[5] Glenzer S.H. *et al* 2010 *Science* **327** 1228
[6] Haan S.W. *et al* 1995 *Phys. Plasmas* **2** 2480
[7] Landen O.L. *et al* 2010 *Phys. Plasmas* **17** 056301
[8] Glenzer S.H. *et al* 1999 *Phys. Plasmas* **6** 2117
[9] Li C.K. *et al* 2010 *Science* **327** 1231
[10] Moses E.I. *et al* 2005 *Fusion Sci. Technol.* **47** 314
[11] Marshall F.J. *et al* 2004 *Phys. Plasmas* **11** 251
[12] Craxton R.S. *et al* 2005 *Phys. Plasmas* **12** 056304
[13] Li C.K. *et al* 2006 *Phys. Rev. Lett.* **97** 135003
[14] Li C.K. *et al* 2008 *Phys. Rev. Lett.* **100** 225001
[15] Rygg J.R. *et al* 2008 *Science* **319** 1223
[16] Petrasso R.D. *et al* 2009 *Phys. Rev. Lett.* **103** 0851001
[17] Li C.K. *et al* 2009 *Phys. Rev. Lett.* **102** 205001
[18] Li C.K. *et al* 2012 *Phys. Rev. Lett.* **108** 025001
[19] Seguin F.H. *et al* 2012 *Phys. Plasmas* **19** 012701
[20] Borghesi M. *et al* 2004 *Phys. Rev. Lett.* **92** 055003
[21] Mackinnon A. *et al* 2006 *Phys. Rev. Lett.* **97** 045001
[22] Hey D.S. *et al* 2008 *Rev. Sci. Instrum.* **79** 053501
[23] Zylstra A.B. *et al* 2012 *Rev. Sci. Instrum.* **83** 10D901
[24] Snavely R.A. *et al* 2000 *Phys. Rev. Lett.* **85** 2945
[25] Robson L. *et al* 2007 *Nature Phys.* **3** 58
[26] Offermann D.T. *et al* 2011 *Phys. Plasmas* **18** 056713
[27] Flippo K. *et al* 2010 *J. Phys.: Conf. Ser.* **244** 022033
[28] Soures J.M. *et al* 1996 *Phys. Plasmas* **3** 2108
[29] Seguin F.H. *et al* 2003 *Rev. Sci. Instrum.* **74** 975
[30] Zimmerman G.B. and Kruer W.L. 1975 *Comments Plasma Phys. Control. Fusion* **2** 51
[31] Nielsen P.D. and Zimmerman G.B. 1981 *Lawrence Livermore National Laboratory Report* No UCRL-53123
[32] Welch D.R. *et al* 2001 *Nucl. Instrum. Methods Phys. Res.* A **464** 134
[33] Meyerhofer D.D. *et al* 2001 *Phys. Plasmas* **8** 2251
[34] Li C.K. *et al* 1993 *Phys. Rev. Lett.* **70** 3059
[35] Braginskii S.I. 1965 *Review of Plasma Physics* vol 1 (New York: Consultants Bureau)
[36] Haines M.G. 1997 *Phys. Rev. Lett.* **78** 254
[37] Manuel M.J.-E. *et al* 2012 *Phys. Rev. Lett.* **108** 255006
[38] Srinivansan B. *et al* 2012 *Phys. Rev. Lett.* **108** 165002
[39] Amendt P.A. *et al* 2009 *Plasma Phys. Control. Fusion* **51** 124048